


## Article

# Effect of Cross-Well Natural Fractures and Fracture Network on Production History Match and Well Location Optimization in an Ultra-Deep Gas Reservoir

Dong Chen <sup>1,2,3,4</sup>, Yuwei Jiao <sup>5</sup>, Fenglai Yang <sup>1</sup>, Chuxi Liu <sup>6</sup>, Min Yang <sup>1</sup>, Joseph Leines Artieda <sup>6</sup> and Wei Yu <sup>6,\*</sup> 

<sup>1</sup> Tarim Oilfield Petrochina, Tarim, Korla 841000, China; chdong-tlm@petrochina.com.cn (D.C.); yangfl-tlm@petrochina.com.cn (F.Y.); yangmin\_tlm@petrochina.com.cn (M.Y.)

<sup>2</sup> R&D Center for Ultra-Deep Complex Reservoir Exploration and Development, CNPC, Tarim, Korla 841000, China

<sup>3</sup> Engineering Research Center for Ultra-Deep Complex Reservoir Exploration and Development, Xinjiang Uygur Autonomous Region, Tarim, Korla 841000, China

<sup>4</sup> Xinjiang Key Laboratory of Ultra-Deep Oil and Gas, Tarim, Korla 841000, China

<sup>5</sup> Research Institute of Petroleum Exploration and Development, Beijing 100083, China; jiaoyuwei@petrochina.com.cn

<sup>6</sup> SimTech LLC., Houston, TX 77084, USA; liu.francis@utexas.edu (C.L.); joseph.leines@simtechnologyus.com (J.L.A.)

\* Correspondence: yuwei127@gmail.com; Tel.: +86-(512)-574-0080

**Abstract:** Understanding subsurface natural fracture systems is crucial to characterize well production dynamics and long-term productivity potential. In addition, the placement of future wells can benefit from in-depth fracture network connectivity investigations, vastly improving new wells' profitability and life cycles if they are placed in dense, well-connected natural fracture zones. In this study, a novel natural fracture calibration workflow is proposed. This workflow starts with the extraction of sector geology and a natural fracture model from the pre-built full-field model. Then, a cross wellbore discrete fracture network (CW-DFN) is created using a novel CW-DFN generation tool, based on image log data. An innovative fracture network identification tool is developed to detect the interconnected regional fracture network (IcFN) with CW-DFN. The non-intrusive embedded discrete fracture model (EDFM) is utilized to numerically incorporate the complex IcFN and CW-DFN in a reservoir simulation, and it is history-matched by tuning their conductivities. This workflow is applied to a single vertical well within a natural fracture carbonate reservoir in Northwest China. The study results show that the number of CW-DFNs is 11, and the number of IcFNs is 72. The non-intersected natural fractures only account for 5.5% of the production, and thus can be removed to improve simulation efficiency. The history-matching absolute average relative deviation (AARD) is 15.16%. The calibrated effective fracture permeability is 280 millidarcy, with an aperture of 0.001 m, equating to a conductivity of 0.28 millidarcy-meter. The 30-year gas production forecast is estimated to be 1.66 billion cubic meters based on a history-matched model. Finally, if the well is drilled to the east of the sector, 30-year production declines to 1.33 billion cubic meters (a reduction of 20%). However, if the well is drilled to the west of the sector, 30-year production increases to 2 billion cubic meters (an improvement of 20.5%).

**Keywords:** embedded discrete fracture model; cross wellbore discrete fracture network (DFN); DFN calibration; well location optimization



**Citation:** Chen, D.; Jiao, Y.; Yang, F.; Liu, C.; Yang, M.; Leines Artieda, J.; Yu, W. Effect of Cross-Well Natural Fractures and Fracture Network on Production History Match and Well Location Optimization in an Ultra-Deep Gas Reservoir. *Processes* **2024**, *12*, 1085. <https://doi.org/10.3390/pr12061085>

Academic Editors: Qingbang Meng, Bin Liang and Zhan Meng

Received: 30 March 2024

Revised: 13 May 2024

Accepted: 23 May 2024

Published: 25 May 2024



**Copyright:** © 2024 by the authors. Licensee MDPI, Basel, Switzerland. This article is an open access article distributed under the terms and conditions of the Creative Commons Attribution (CC BY) license (<https://creativecommons.org/licenses/by/4.0/>).

## 1. Introduction

Naturally fractured reservoirs, holding nearly 40% of the world's gas reserves [1], pose significant challenges for the oil and gas industry due to their complex fracture networks. These networks play a crucial role in fluid dynamics and, consequently, in the performance of reservoirs. Given the substantial uncertainties surrounding natural fracture distribution, accurate modeling and simulation become essential for optimizing extraction processes.

To achieve detailed characterization of natural fractures, industry professionals rely on static borehole images (BHI), core, seismic, and outcrop data [2–4]. The connectivity formed by these natural fractures, a vital determinant of well performance, is influenced by fracture geometry and density. Notably, denser and longer fractures tend to facilitate greater connectivity than their shorter and sparser counterparts [5]. This connectivity, especially when fractures intersect the wellbore trajectory, significantly impacts well performance.

Dynamic production and well-testing data are crucial for calibrating properties such as fracture permeability, porosity, and geometries [6–9]. This often involves an iterative process to refine the uncertain attributes of natural fractures [10], reducing the uncertainties in discrete fracture network (DFN) characterization. Calibrated DFN models are invaluable for predicting pressure depletion and optimizing new well developments.

The traditional dual porosity dual permeability (DPDK) method, despite its widespread application for reservoir simulation and history matching [11–13], struggles with explicit single fracture modeling and tends to overestimate natural fracture connectivity [14–18]. Such methods inaccurately assume disconnected fractures to be connected networks [5,19]. Although local grid refinement and unstructured gridding offer alternatives, they are often too time-intensive for simulating complex three dimensional (3D) natural fractures [20,21].

To address these challenges, the embedded discrete fracture method (EDFM) has been developed, offering a robust solution to explicitly model individual natural fractures [22–24]. However, the effects of natural fracture connectivity on well performance and the process of fracture calibration remain underexplored.

This study introduces a novel workflow for DFN calibration and validation using production data, examining the connectivity between natural fractures and the wellbore through the EDFM method. Our approach can handle 3D DFN models of any geometry, orientation, and dip angle, ensuring full capture of the interaction between the DFN and the geology model. A field application demonstrates the workflow's ability to calibrate DFN properties effectively, examining their impacts on well performance and achieving a satisfactory match between simulation results and production data. This calibrated DFN model also facilitates an investigation into the effects of new well locations based on performance, underscoring our workflow's capability to characterize reservoir dynamics comprehensively.

## 2. Methodology

The proposed single-well DFN calibration methodology is described below (Figure 1). First, the full-field reservoir model and fracture model is obtained. These models are either cut, refined, or extracted to form a sector model that only contains the well of study. Alongside this step, original image log data are obtained for the well, and the cross-wellbore DFN generation module is utilized to create fractures that are intersecting the wellbore. Then, a DFN analyzer is implemented to identify a connected fracture network between sector DFN and generated cross-wellbore DFN. Reservoir simulation is then carried out with the help of EDFM. If the DFN network does not match the history production, another cross-wellbore DFN will be generated, but with a different fracture size. Then, the network identification is repeated, until history data can be matched. We then obtain the history-matched model and production forecast will be studied using the representative DFN network model to quantify long-term estimated ultimate recovery (EUR).

### 2.1. Cross-Wellbore DFN Generation

Cross-wellbore fractures are generated using standard well image logs, in which measured depth, azimuth angle, dip angle, and interpretation status are used as inputs. Interpretation status measures whether the natural fracture is conductive (it has certain apertures) or sealed (it is cemented).

Each natural fracture is subjected to its own coordinate system as a function of its azimuth and dip angle. In order to define a natural fracture using this coordinate system, we define three vectors: azimuth, dip, and normal vector Equations (1)–(3).

$$n_a = [\cos(\text{azimuth}) \quad \sin(\text{azimuth}) \quad 0] \quad (1)$$

$$n_d = [-\sin(\text{azimuth}) \cos(\text{dip}) \quad \cos(\text{azimuth}) \cos(\text{dip}) \quad \sin(\text{dip})] \quad (2)$$

$$n_n = [-\sin(\text{azimuth}) \sin(\text{dip}) \quad \cos(\text{azimuth}) \sin(\text{dip}) \quad -\cos(\text{dip})] \quad (3)$$

where  $n_a$  is the azimuth vector,  $n_d$  is the dip vector, and  $n_n$  is the normal vector; azimuth and dip are the azimuth and dip angles of the natural fracture.

We assumed a natural fracture intersects the well trajectory at the center of its polygonal representation. The polygon center coordinate can be interpolated based on its measured depth from the well trajectory. Then, by assigning the required fracture length and height, one can generate the polygon vertices' coordinates based on the defined coordinate system, as shown in Figure 2.

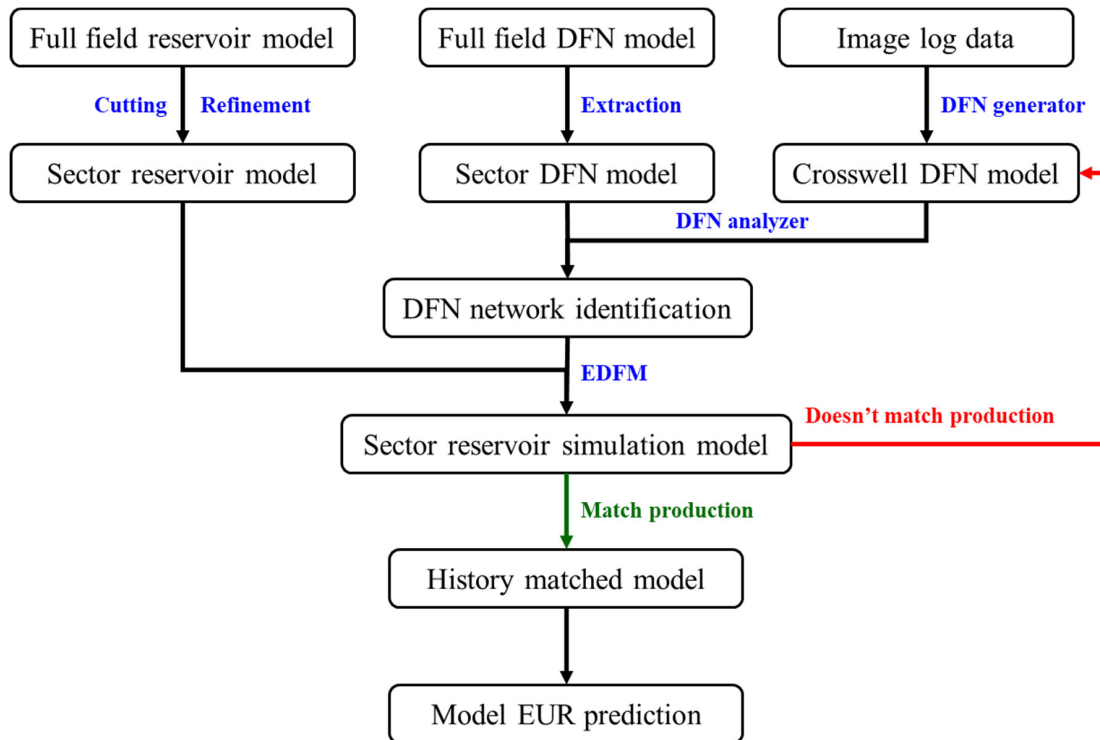


Figure 1. Single-well sector model DFN calibration workflow.

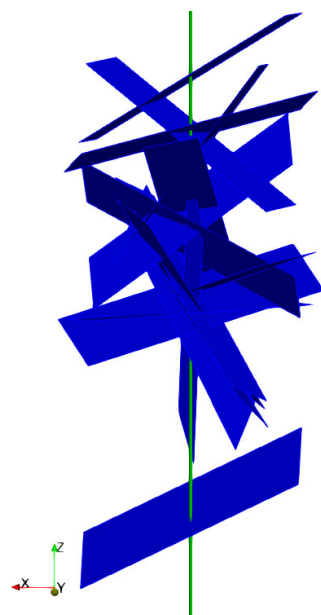
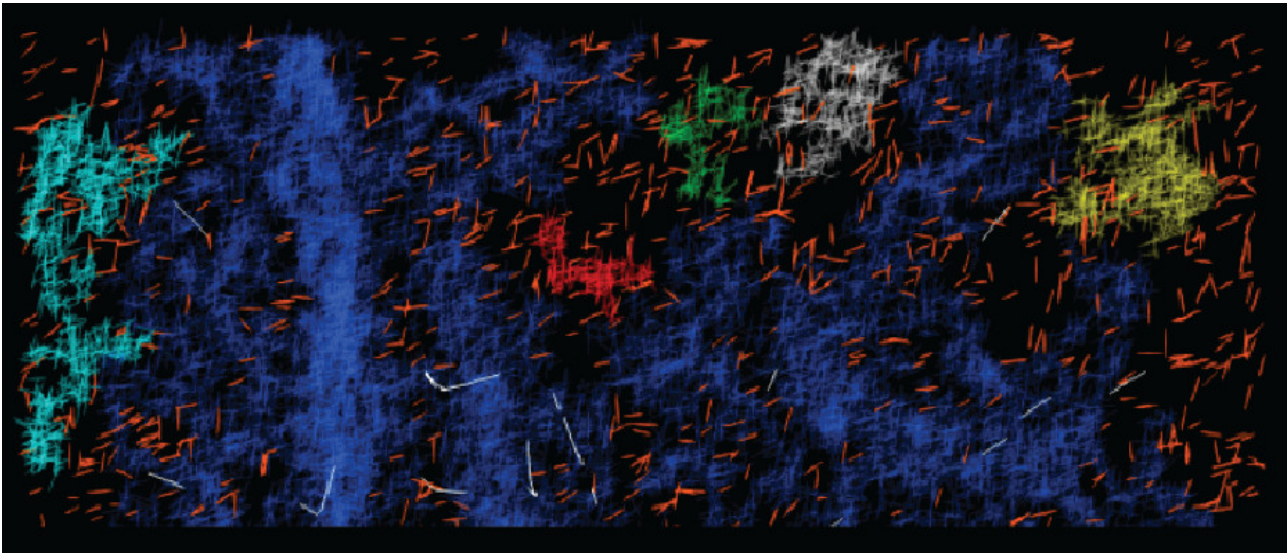


Figure 2. Schematic of a well trajectory intersecting cross-wellbore natural fractures.

## 2.2. Fracture Network Identification

Fracture network identification was achieved by using a collision detection algorithm [25], which models the fracture network as a series of 3D polygons. The algorithm is capable of detecting all groups of connected natural fractures from a file containing only their spatial coordinates. Figure 3 shows the identification of six natural fracture groups, highlighting the blue group as the largest one and the orange group as the one with disconnected fractures.



**Figure 3.** Schematic of fracture network identification results.

The DFN identification process starts by including the original DFN model. Then, we generate the cross-wellbore DFN based on image log data. We combine both DFN models and run the collision detection algorithm to extract the groups of connected fractures. Finally, we search inside the connected groups that include the cross-wellbore fractures to generate a network of natural fractures that directly connect with the cross-wellbore fractures.

This process maximizes the operator's available data usage because it incorporates direct measurements from well image logs to support the history-matching process.

## 2.3. Embedded Discrete Fracture Model (EDFM)

Conventional reservoir simulations in fractured reservoirs cannot benefit from robust reservoir characterization methods such as cross-wellbore generation and fracture network identification because they treat the fracture network as a whole. By using traditional dual porosity methods to incorporate the effect of a fracture network, the modeler loses key spatial data and ends up overestimating the effect of the natural fracture network. In contrast, EDFM can explicitly model 3D natural fractures and can capture more realistic scenarios, such as connected fracture networks [22]. In addition, EDFM provides superior flexibility when it comes to running additional sensitivity studies where the main variables to be studied are spatial properties (natural fracture orientation, density, and geometry).

EDFM embeds each fracture inside the matrix grid, and its effects on production are quantified by their connections with the matrix, other natural fractures, and portions of the fracture itself located in different matrix grid blocks. These connections are modeled by adding new cells to the computational domain whose main calculations are done by using non-neighboring connections (NNCs) in traditional reservoir simulators.

### 3. Field Application of DFN Analysis

#### 3.1. General Reservoir Model

The proposed DFN analysis workflow is implemented in a region of a naturally fractured carbonate gas reservoir (short named DB) in Northwest China. There are a total of four vertical wells that have been put into production. As can be seen in Figure 4, the full-field reservoir model covers an area of 20 km long, 1.8 km wide, and 240 m thick. The original model grid block size is 100 m  $\times$  100 m  $\times$  2.1 m in x, y, and z directions. Well-4 is selected to demonstrate the workflow, and the single-well sector model is cut and refined. The sector model covers an area of 2.3 km  $\times$  1.7 km with the same thickness, with a higher horizontal grid resolution of 20 m. The sector model's depth ranges from 3370 to 3612 m, and the porosity, permeability, water saturation, and pressure heterogeneity maps are plotted in Figure 5; the statistical histogram of these properties' distributions are plotted in Figure 6. The average values for these properties are 4%, 0.32 md, 40%, and 81 MPa. The standard deviations (STD) of these properties are 2.9%, 0.48 md, 27%, and 0.36 MPa. Detailed model information can be found in Table 1. From Figure 6, we can observe that the porosity and water saturation exhibit right-skewed distribution with the mode at 3.75% and 42.5%, respectively. The permeability exhibits flipped lognormal distribution with its mode at 0.4 md. The pressure exhibits normal distribution with its mode at 81.5 MPa.

**Table 1.** Basic properties of the full-field and sector gas reservoir model.

Properties	Value	Unit
Full-field model dimension (x $\times$ y $\times$ z)	20 $\times$ 1.8 $\times$ 240	km $\times$ km $\times$ m
Full-field number of grid blocks (x $\times$ y $\times$ z)	202 $\times$ 23 $\times$ 118	-
Full-field grid cell size (x $\times$ y $\times$ z)	100 $\times$ 100 $\times$ 2.1	m $\times$ m $\times$ m
Sector model dimension (x $\times$ y $\times$ z)	2.3 $\times$ 1.7 $\times$ 240	km $\times$ km $\times$ m
Sector number of grid blocks (x $\times$ y $\times$ z)	115 $\times$ 85 $\times$ 118	-
Sector grid cell size (x $\times$ y $\times$ z)	20 $\times$ 20 $\times$ 2.1	m $\times$ m $\times$ m
Reservoir depth range	3370~3612	m
Average/STD of porosity	4/2.9	%
Average/STD of permeability	0.32/0.48	md
Average/STD of water saturation	40/27	%
Average/STD of reservoir pressure	81/0.36	MPa

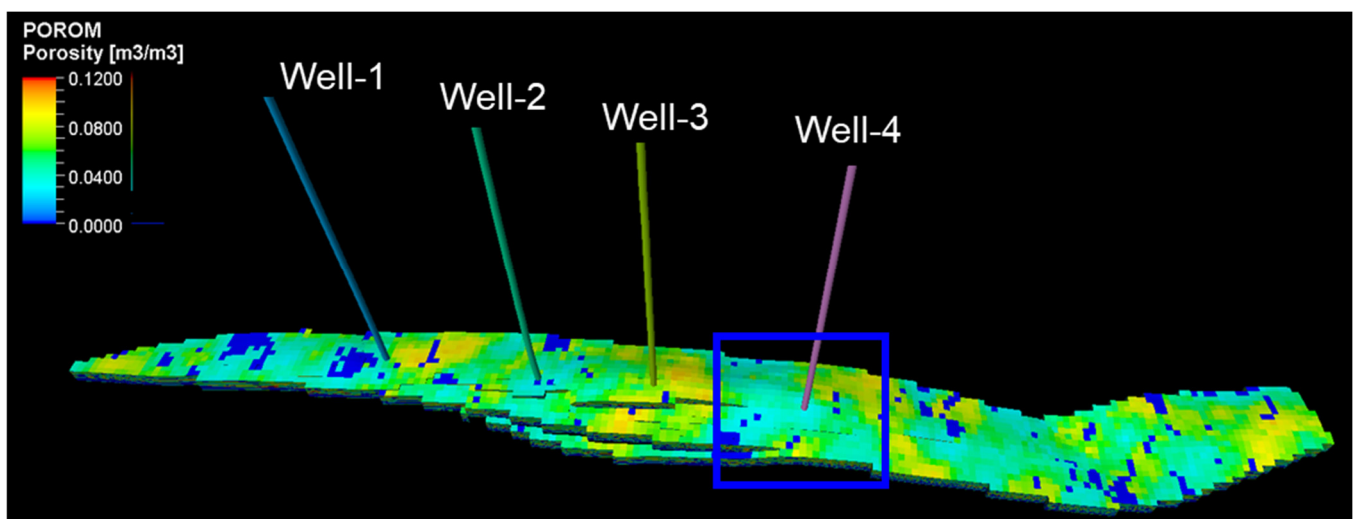


**Figure 4.** Full-field view of the gas reservoir's porosity heterogeneity.

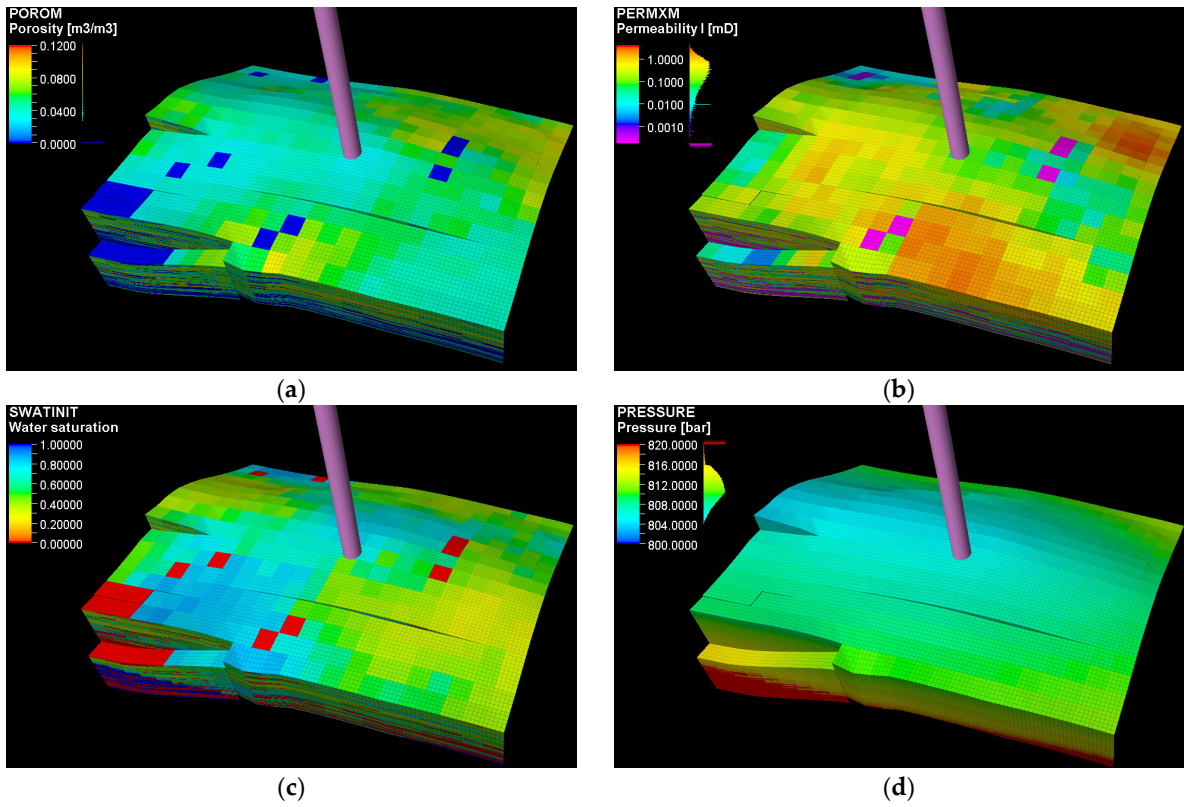


Figure 5. Sector view of the single-well model's petrophysical properties: (a) porosity; (b) permeability; (c) water saturation; (d) reservoir pressure.

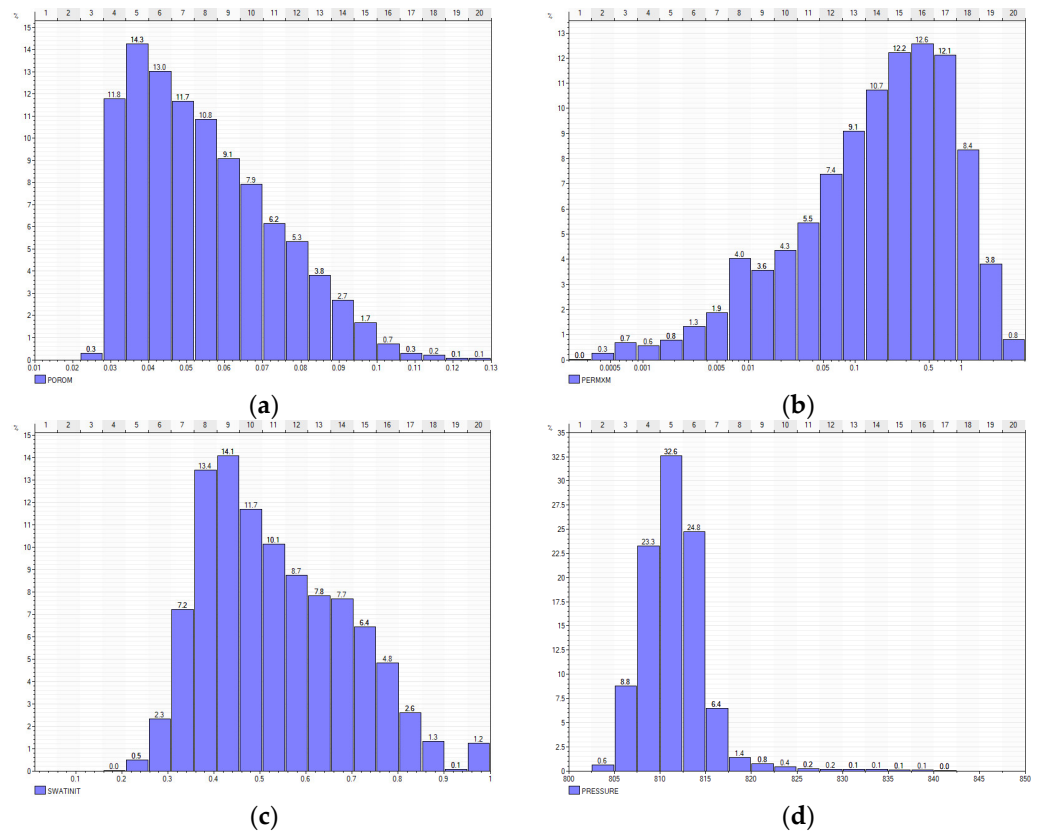


Figure 6. Statistical distributions of the single-well model's petrophysical properties: (a) porosity; (b) permeability; (c) water saturation; (d) reservoir pressure.

### 3.2. In Situ DFN Model and Cross Wellbore DFN Model

A 3D in situ DFN model was constructed using regional knowledge and overall image log statistics such as fracture intensity. The total number of full-field DFNs is 1 million (See Figure 7). Based on the areal extent of the sector reservoir model, the sector DFN model was extracted (Figure 8). The number of fractures within the sector model is 116 thousand. The average azimuth has two major trends, orienting at 107 and 285 degrees (STD is 68.5°), with a single dip trend averaging 77 degrees and a STD of 7.6 degrees. The average fracture length is 77 m, and the STD is 12.9 m. The mean and STD of fracture height is 40 m and 6.7 m. Table 2 tabulates detailed information about the in situ DFN model.

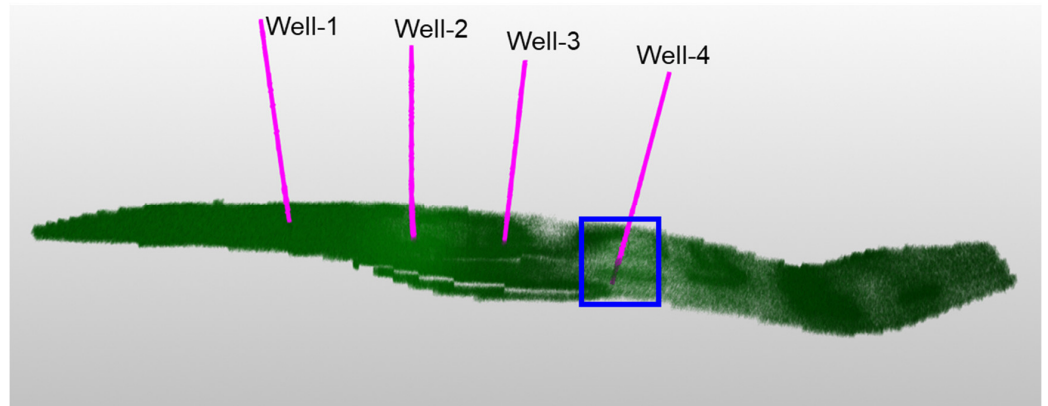


Figure 7. Full-field DFN model.

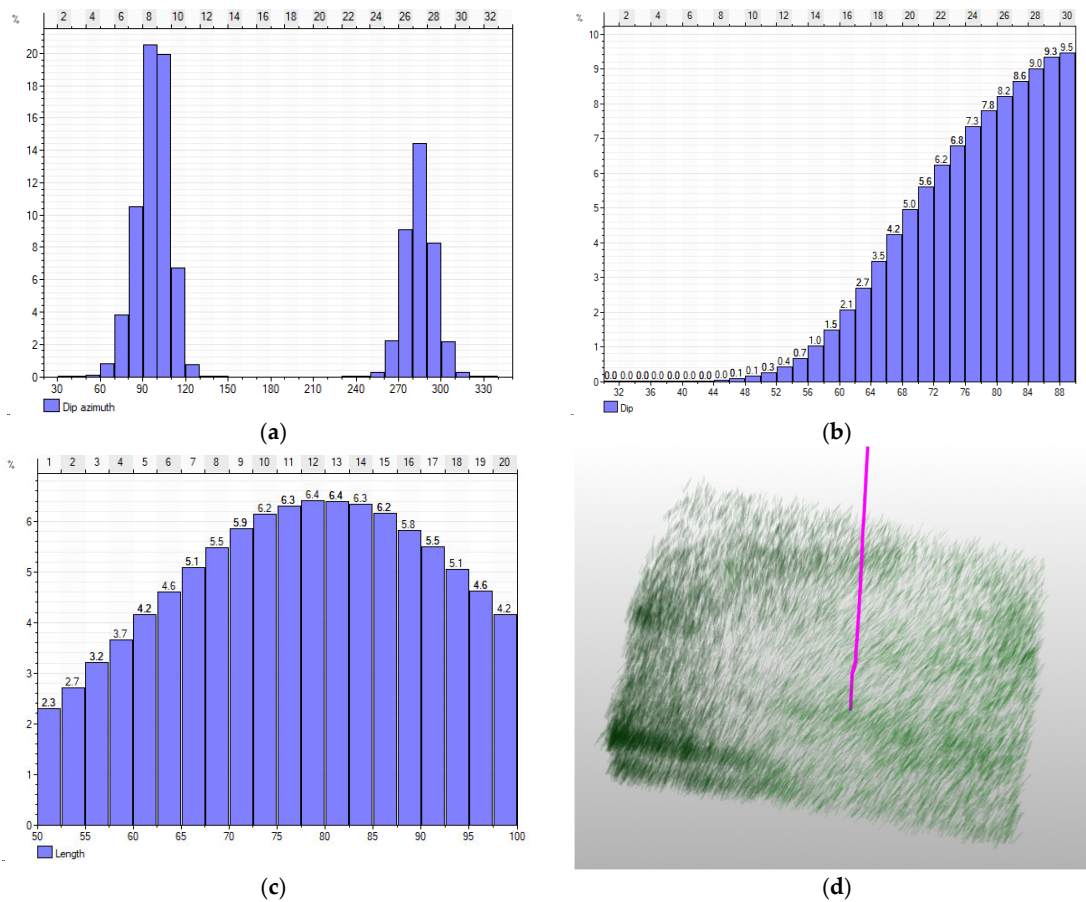
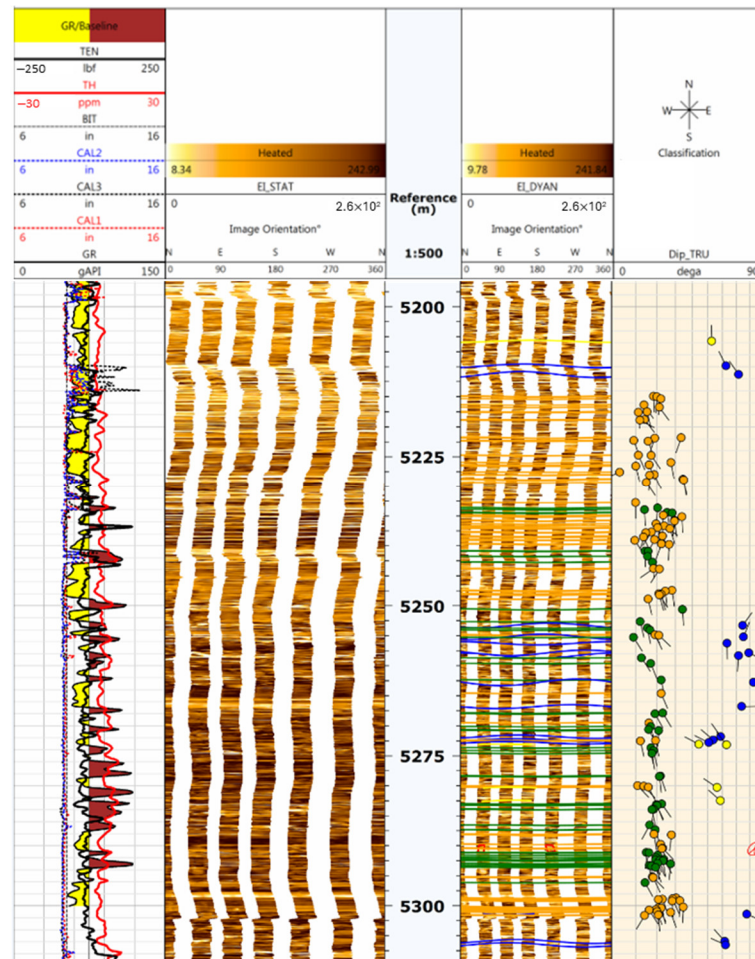


Figure 8. Spatial configuration of the DFN model and the extracted sector DFN model. (a) Azimuth angle distribution histogram; (b) dip angle distribution histogram; (c) DFN length distribution histogram; and (d) extracted sector DFN.

**Table 2.** Basic properties of the DFN model within this gas reservoir.

Properties	Value	Unit
Full-field DFN number	1 million	-
Sector DFN number	22,330	-
Average azimuth angle (2 sets), STD of azimuth	107/285, 68.5	°
Average/STD of dip angle	77/7.6	°
Average/STD length	77/12.9	m
Average/STD height	40/6.7	m

By using the well-based image log data (Figure 9), a cross-wellbore DFN was then created. Fracture azimuth and dip information were directly obtained from the tad-pole plots. For the base case, the length of the cross-wellbore DFN follows power-law distribution with a power-law constant of 30 m, a maximum of 100 m, and a power-law exponent of 1.5. The height of the cross-wellbore DFN follows uniform distribution, which was randomly sampled between 15 m and 25 m. A total of 11 cross-wellbore DFNs were created. The generated base case cross-wellbore DFN is shown in Figure 10.

**Figure 9.** Original image log data input for cross-well DFN generation.



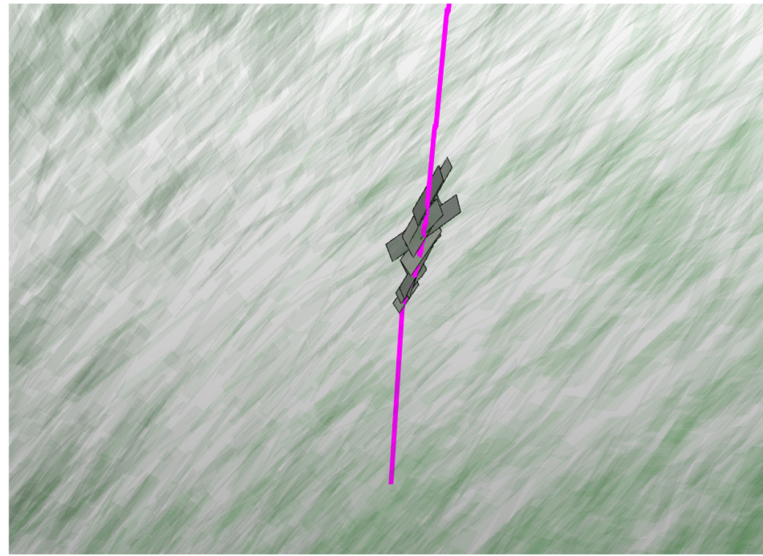


**Figure 10.** Base case cross-well DFN model.

### 3.3. DFN Network Identification

The next step was to identify the DFN networks, which are a subset of the sector DFN that both intersect the cross-well DFN and are connected to each other. Figure 11 shows the network identified by the algorithm, which is highlighted in transparent blue. In this case, a total of 72 DFNs are identified as the intersecting network.

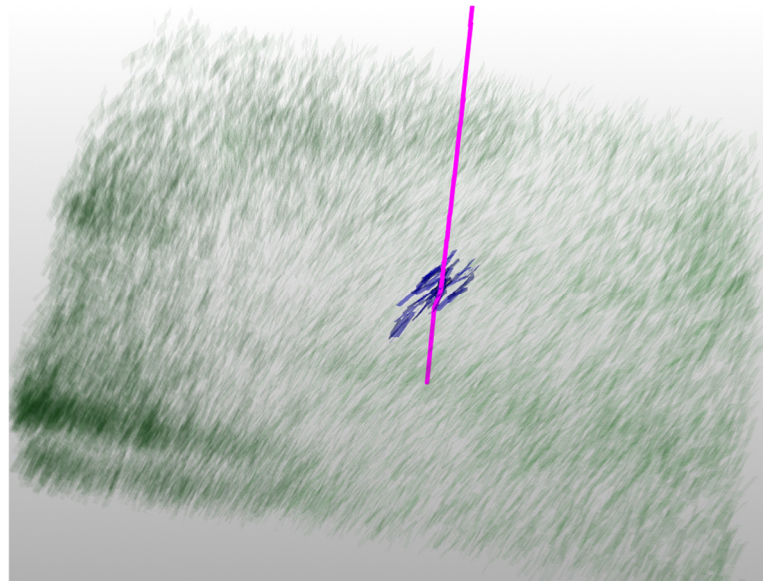


**Figure 11.** Intersected DFN network model, highlighted by transparent blue.

## 4. Reservoir Simulation and History Matching

Based on core data (Figure 12), image log analysis (Figure 13), and well-testing results (Table 3), the reservoir area near Well-4 is characterized with low leak-off (12 cubic meters from well test), a high degree of calcite fillings, and highly ineffective fracture networks (0% of open fracture, 75% of semi-open fractures, and 25% closed fractures). Compared with image log analysis for other wells (15%, 64%, and 87% of open fractures for Well-1, Well-2, and Well-3), we believe that the effective equivalent fracture conductivity will be low.

Traditionally, the single-well model is calibrated using the gas flow rate as the operating constraint, and bottomhole pressure (BHP) is the matching target. However, the calculated BHP history data of this well show half of the initial reservoir pressure, right

after the well starts producing. The variation of BHP is also pretty small after almost 3 years of production. Therefore, the strategy to use BHP as a well constraint and to set cumulative gas production as a matching target was adopted. Figure 14 shows the BHP history (black circle) of this well versus the initial reservoir pressure (red dash).



Figure 12. Core data observations of calcite filling across different wells in the reservoir.

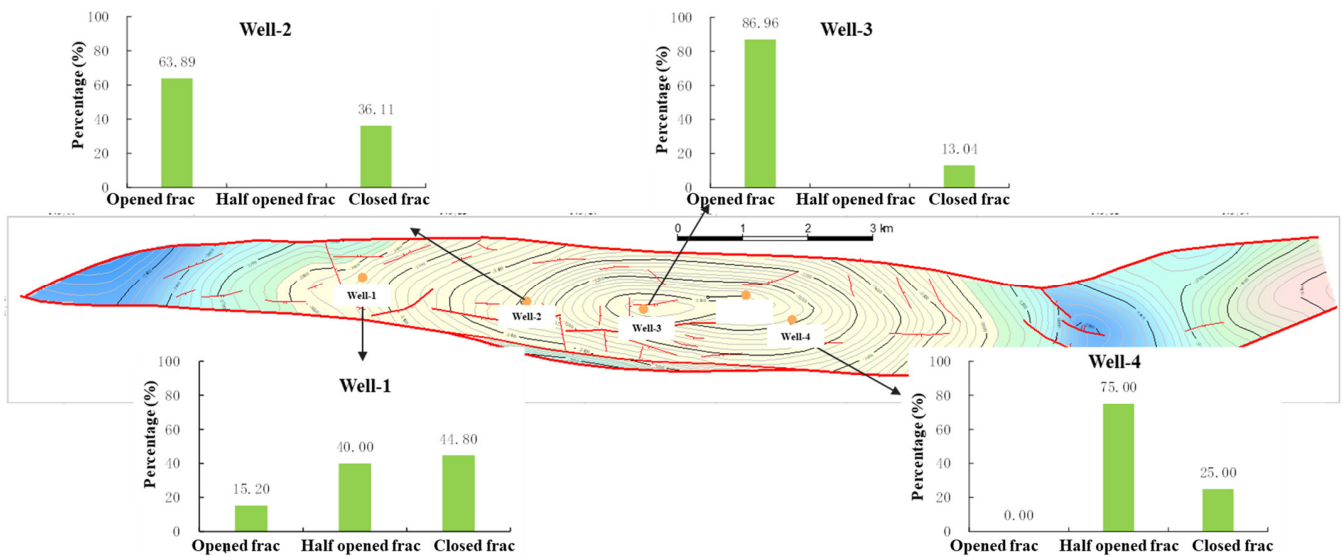


Figure 13. Image log analysis across different wells in the reservoir.

Table 3. Well-testing results across different wells in the reservoir.

Well Name	Leak-Off Volume (m <sup>3</sup> )	Matrix Permeability (md)
Well-1	98.8	-
Well-2	10.94	5.91
Well-3	157.07	8.56
Well-4	11.8	0.17

The base case reservoir simulation was run with and without a non-intersected DFN network, and the results are shown in Figure 15. As can be seen, cumulative gas production has minimal differences (5.5% apart) for the period of the production history. Therefore, the history-matching process can be done without considering non-intersected networks to speed up the matching. After tuning the fracture network conductivity, the best match

was achieved as shown in Figure 16. The history-matching accuracy of cumulative gas production, quantified by absolute average relative deviation (AARD), was calculated to be 15.16%. The representative fracture aperture and permeability were 1 mm and 280 md, equivalent to a conductivity of 0.28 md-m. Figure 17 shows the predicted 30-year long-term production of gas, using the history-matched model. For the prediction period, the bottomhole pressure declines linearly, similar to the trends of the last 30 days of history bottomhole pressure, until it reaches a minimum of 10 MPa. The value of 10 MPa is chosen because this is the empirical value often used by the operator. This value represents the maximum physically possible drawdown by the well. Any value above this does not maximize long-term production, and any value below this will require additional manually supplied energy (such as pumps) and will add cost. The estimated ultimate recovery (EUR) is approximately 1.66 billion cubic meters.

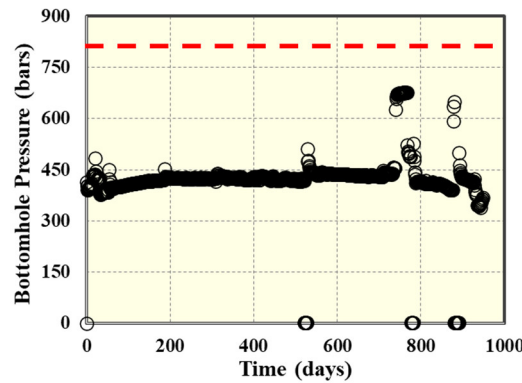


Figure 14. Well-4's BHP history (black circle) and average initial reservoir pressure (red dash).

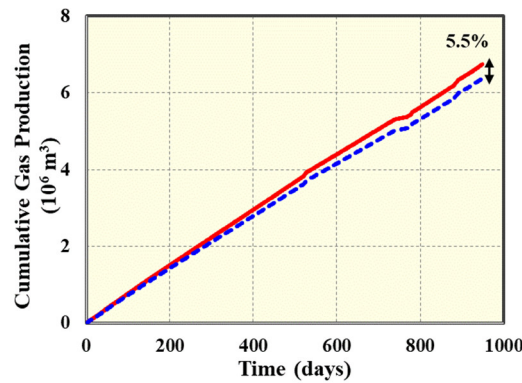


Figure 15. Base case cumulative gas production with and without non-intersected DFN.

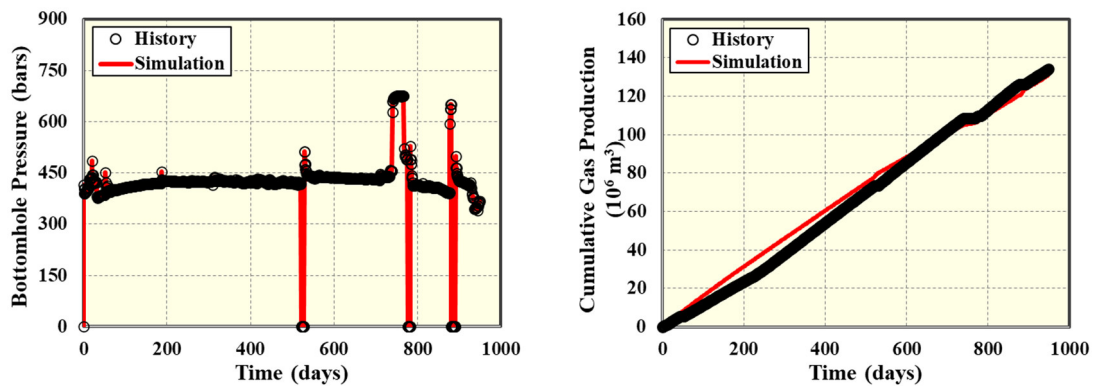


Figure 16. Bottomhole pressure constraint (left) and history-matched cumulative gas production (right).

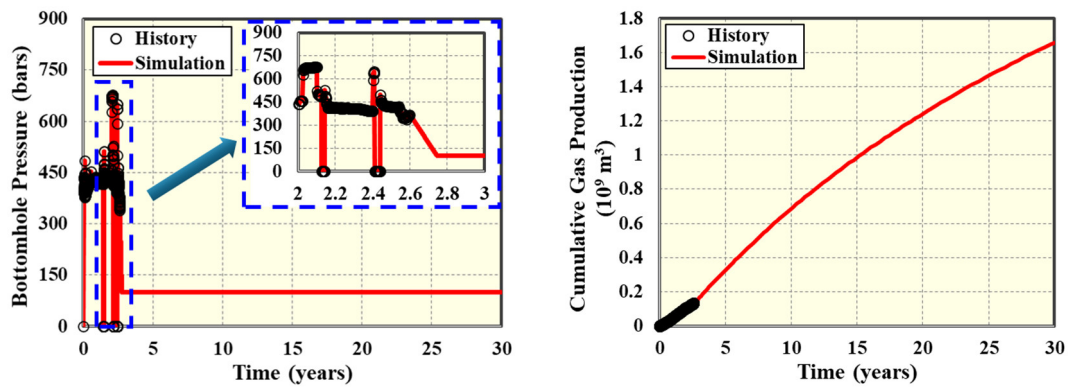


Figure 17. The 30-year gas EUR prediction (right) using minimum bottomhole pressure of 10 MPa (left).

### 5. Well Location Optimization

Based on the observations from cross-well DFN generation, network identification, and history matching, the well performance potential of the current well drilling location could be optimized. This is feasible because the DFN intensity is much higher in the western region of the sector model than the eastern part. Therefore, two new well drilling locations are proposed to study the well location's impact on the long-term well performance. Figure 18 shows the proposed location (purple) and also the detected DFN network (blue), assuming the same configuration of the cross-well DFN. The reservoir simulations for these two well location scenarios were performed (assuming same DFN conductivity as calibrated value), and Figure 19 displays the 30-year cumulative gas production. It was observed that if the well is drilled to the east of the sector, there will be a total of 55 natural fractures intersecting the 11 cross-well DFN, and the 30-year EUR will decline to 1.33 billion cubic meters, or a 20% reduction. However, if the well is drilled to the west, there will be a total of 11,416 natural fractures intersecting the 11 cross-well DFN, and the 30-year EUR will be improved to 2 billion cubic meters (20.5% increase). Therefore, it is suggested that future wells should be planned in the western region of this sector. Figure 20a–c shows the 5-year, 15-year, and 30-year matrix/fracture pressure distributions with original well drilling location. The average fluid pressure within the matrix drops to approximately 500 bars after 30 years of production. The comparisons of pressure distributions with different well drilling location after 5 years, 15 years, and 30 years are plotted in Figure 20d–i. Compared with the original well location, we can see that the degree of drainage is suboptimal if the well is drilled to the east (average fluid pressure only drops to 550 bars after 30 years), but will be maximized if the well is drilled to the west (average fluid pressure can drop to 450 bars after 30 years).

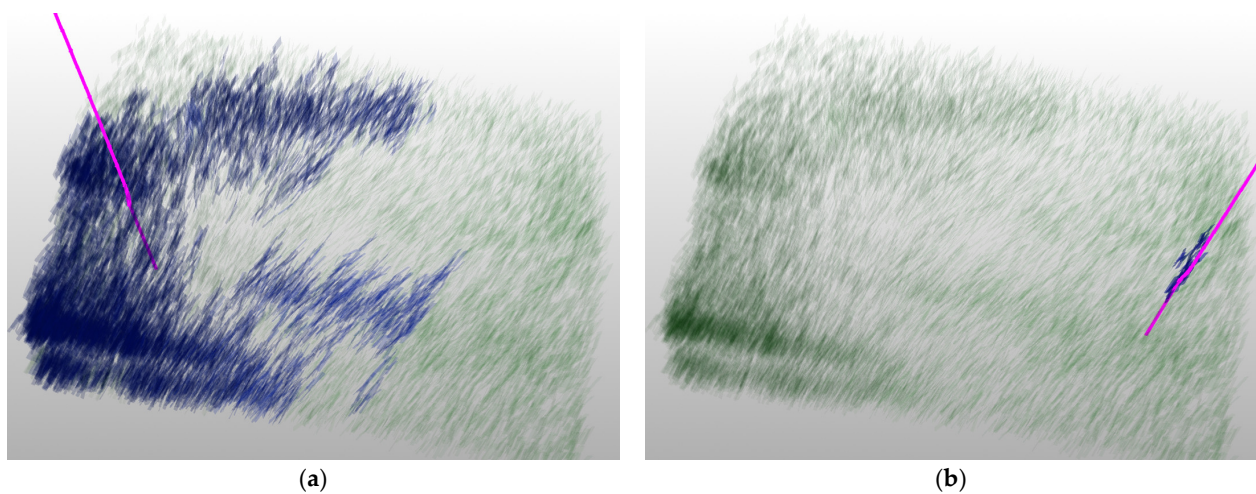


Figure 18. Horizontal cross-section of pressure distribution at different periods of production. (a) Well drilling location moved to the west; (b) well drilling location moved to the east.

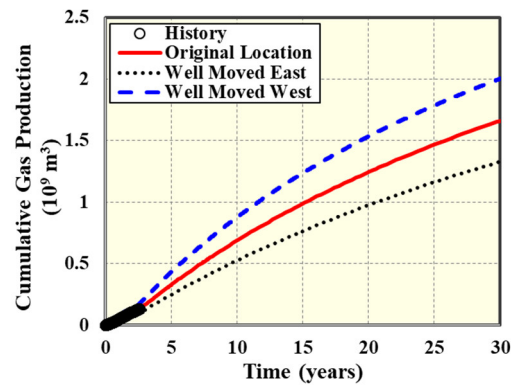


Figure 19. Horizontal cross-section of pressure distribution at different periods of production.

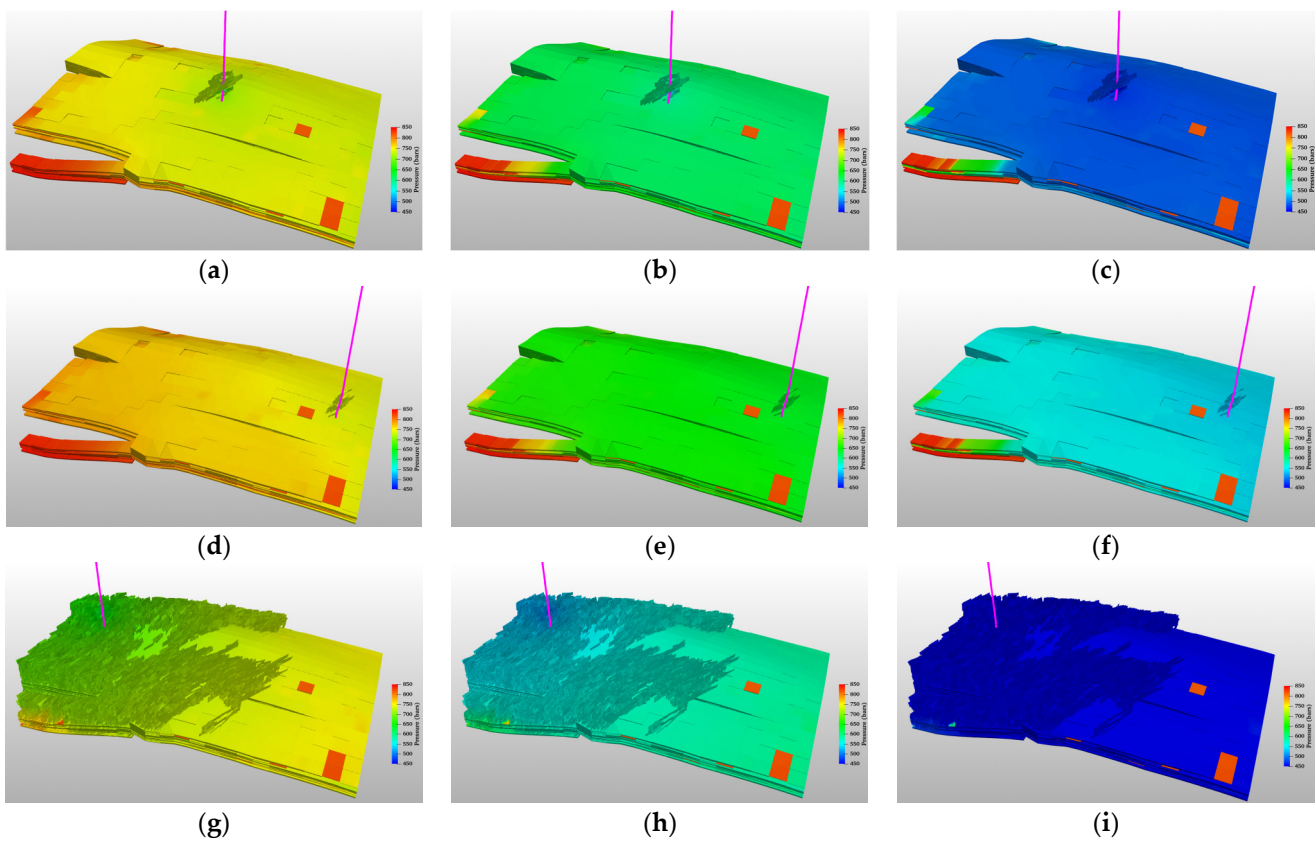


Figure 20. Horizontal cross-section of pressure distribution at different periods of production for different well location scenarios, within the matrix and fractures. (a) After 5 years of production, original well drilling location; (b) after 15 years of production, original well drilling location; (c) after 30 years of production, original well drilling location; (d) after 5 years of production, well drilled to east; (e) after 15 years of production, well drilled to east; (f) after 30 years of production, well drilled to east; (g) after 5 years of production, well drilled to west; (h) after 15 years of production, well drilled to west; (i) after 30 years of production, well drilled to west.

## 6. Conclusions

An innovative DFN analysis workflow was applied successfully to a field case carbonate reservoir, in which a single well's DFN network was calibrated through production history. The cross wellbore DFN (CW-DFN) was generated using the comprehensive image log data, and DFN network was identified with the generated CW-DFN and a pre-built regional DFN model. The conductivity of this DFN network was evaluated with history matching, and a 30-year gas EUR forecast was modelled to quantify well performance.

Lastly, using this workflow, we were able to propose an optimized well drilling location for future development. The following are the detailed summaries:

- (1) By incorporating image log data, the CW-DFN can be created with ease. The network identification tool is robust to assess the connectivity of the regional DFN with CW-DFN. The DFN conductivity has high uncertainty, but can be calibrated by history matching with help of EDFM, and is finally quantified to be 0.28 md-m.
- (2) With EDFM, the long-term well performance can be appraised. The 30-year gas EUR is estimated to be 1.66 billion cubic meters.
- (3) With the DFN network identification tool, the well drilling location has space for optimization. It is suggested that new wells should target the western part of this sector model, as the DFN intensity is higher and CW-DFN can be connected to a system of more than 11 thousand natural fractures. Thirty-year gas production can be improved potentially by 0.34 billion cubic meters (from 1.66 to 2 billion cubic meters), or a 20% increase.
- (4) Based on the pressure drainage visualization, we observe that the original well location, well drilled to the east of sector, and well drilled to the west of the sector will reach average fluid pressures of 50 MPa, 55 MPa, and 45 MPa, respectively.

**Author Contributions:** Conceptualization, D.C. and W.Y.; methodology, Y.J.; validation, F.Y.; investigation, C.L. and J.L.A.; writing—original draft preparation, D.C.; writing—review and editing, C.L. and M.Y. All authors have read and agreed to the published version of the manuscript.

**Funding:** We acknowledge the financial support by Research on New Mechanisms and Methods for Enhancing Recovery in Condensate Gas Reservoirs (2023ZZ0406) and Research on Dynamic Monitoring Methods and Diagnostic Techniques for HTHP Gas Reservoirs (2021DJ1006).

**Data Availability Statement:** The data underlying the results presented in this paper are not publicly available at this time, but may be obtained from the authors upon reasonable request.

**Conflicts of Interest:** Authors Dong Chen, Fenglai Yang and Min Yang were employed by the company Tarim Oilfield Petrochina. Authors Chuxi Liu, Joseph Leines Artieda and Wei Yu were employed by the company SimTech LLC. The remaining authors declare that the research was conducted in the absence of any commercial or financial relationships that could be construed as a potential conflict of interest.

## Abbreviations

### Major SI Metric Units and Field Units Conversion Factors

1 meter (m)	=	3.28084	feet (ft)
1 square meters (m <sup>2</sup> )	=	10.76391	square feet (ft <sup>2</sup> )
1 square meters (m <sup>2</sup> )	=	1.01325 × 10 <sup>15</sup>	millidarcy (md)
1 square meters (m <sup>2</sup> )	=	1.01325 × 10 <sup>21</sup>	nanodarcy (nd)
1 mega Pascal (MPa)	=	10	Atmospheric pressure (bars)
1 mega Pascal (MPa)	=	1000	kilo Pascal (kPa)
1 kilo Pascal (kPa)	=	0.14504	pound-force per square inch (psi)
1 kilo Pascal second (kPa·s)	=	1.0	centi Poise (cp)

## References

1. Ahmed, T. Fractured Reservoirs. In *Reservoir Engineering Handbook*; Gulf Professional Publishing: Houston, TX, USA, 2010.
2. Fiallos-Torres, M.; Wang, H.; Yu, W.; Kong, X.; Chen, P.; Xie, H.; Li, N.; Miao, J.; Chen, Z. A New Discrete Fracture Network Calibration Workflow using EDFM Method. In Proceedings of the 54th US Rock Mechanics/Geomechanics Symposium, Golden, CO, USA, 28 June–1 July 2020. Paper ARMA 20-1424.
3. Earnest, E.; Playton, T.; Vitel, S.; Hui, R. Discrete Fracture Network Modeling of a Giant, Naturally Fractured Carbonate Reservoir, Korolev Field, Kazakhstan. In Proceedings of the 3rd International Discrete Fracture Network Engineering Conference, Santa Fe, NM, USA, 29 June–1 July 2022. Paper ARMA 22-0041.
4. Colombi, N.; Bigoni, F.; Colin, R.; Bombaci, F.; Giamminonni, D.; Spaggiari, L.; Mattonelli, V. Data Integration for Fracture Model Characterization in a Middel East Carbonate Reservoir. In Proceedings of the ADIPEC, Abu Dhabi, United Arab Emirates, 2–5 October 2023. Paper SPE 216765.

5. Richard, P.; Lamine, S.; Pattnaik, C.; Al Ajmi, N.; Kidambi, V.; Narhari, R.; LeVarlet, X.; Swaby, P.; Dashti, Q. Integrated Fracture Characterization and Modeling in North Kuwait Carbonate Reservoirs. In Proceedings of the Abu Dhabi International Petroleum Exhibition and Conference, Abu Dhabi, UAE, 13–16 November 2017. Paper SPE 188185.
6. Bourdet, D.; Gringarten, A.C. Determination of Fissure Volume and Block Size in Fractured Reservoirs by Type-Curve analysis. In Proceedings of the SPE Annual Technical Conference and Exhibition, Dallas, TX, USA, 21–24 September 1980. Paper SPE 9293.
7. Eslamloueyan, R.; Vaferi, B.; Ayatollahi, S. Fracture Characterizations from Well Testing Data Using Artificial Neural Networks. In Proceedings of the 72nd EAGE Conference and Exhibition Incorporating SPE EUROPEC 2010, Barcelona, Spain, 14–17 June 2010.
8. Vaferi, B.; Eslamloueyan, R.; Ayatollahi, S. Application of Recurrent Networks to Classification of Oil Reservoir Models in Well-testing Analysis. *Energy Sources Part A Recovery Util. Environ. Eff.* **2015**, *37*, 174–180. [[CrossRef](#)]
9. Ibragimov, A. Reservoir Characterization of a Naturally Fractured Reservoir Using Well Test Data Interpretation. In Proceedings of the SPE Annual Caspian Technical Conference, Nur-Sultan, Kazakhstan, 15–17 November 2022. Paper SPE 212068.
10. Wang, C.J.; Szczurowski, R.; Vecchiarelli, A. DFN Model Validation and Input Parameter Calibration for Hawkesbury Sandstone. In Proceedings of the 54th US Rock Mechanics/Geomechanics Symposium, Golden, Colorado, USA, 28 June–1 July 2020. Paper ARMA 20-1360.
11. Warren, J.E.; Root, P.J. The Behavior of Naturally Fractured Reservoirs. *SPE J.* **1963**, *3*, 245–255. [[CrossRef](#)]
12. Kazemi, H.; Merrill, L.S.; Porterfield, K.L.; Zeman, P.R. Numerical Simulation of Water-Oil Flow in Naturally Fractured Reservoirs. *SPE J.* **1976**, *16*, 317–326. [[CrossRef](#)]
13. Elfeel, A.M. Improved Upscaling and Reservoir Simulation of Enhanced Oil Recovery Processes in Naturally Fractured Reservoirs. Ph.D. Dissertation, Heriot-Watt University, Edinburgh, UK, 2014.
14. Long, J.C.S.; Witherspoon, P.A. The Relationship of the Degree of Interconnection to Permeability in Fracture Networks. *J. Geophys. Res. Solid Earth* **1985**, *90*, 3087–3098. [[CrossRef](#)]
15. Dershowitz, B.; Lapointe, P.; Eiben, T.; Wei, L. Integration of Discrete Feature Network Methods with Conventional Simulator Approaches. *SPE Reserv. Eval. Eng.* **2000**, *3*, 165–170. [[CrossRef](#)]
16. Garcia, M.H.; Gouth, F.M.; Gosselin, O.R. Fast and Efficient Modeling and Conditioning of Naturally Fractured Reservoir Models Using Static and Dynamic Data. In Proceedings of the EUROPEC/EAGE Conference and Exhibition, London, UK, 11–14 June 2007. Paper SPE 107525.
17. Vo, H.; Kamath, J.; Hui, R. High Fidelity Simulation of Recovery Mechanisms in Complex Natural Fracture Systems. In Proceedings of the SPE Reservoir Simulation Conference, Galveston, TX, USA, 10–11 April 2019. SPE 193864.
18. Chen, P.; Fiallos-Torres, M.; Xing, Y.; Yu, W.; Guo, C.; Leines Artieda, J.; Cheng, M.; Xie, H.; Shi, H.; Mao, Z.; et al. Water Intrusion Characterization in Naturally Fractured Gas Reservoir Based on Spatial DFN Connectivity Analysis. *Energies* **2020**, *13*, 4235. [[CrossRef](#)]
19. Oda, M. Permeability Tensor for Discontinuous Rock Masses. *Geotech. J.* **1985**, *35*, 483–495. [[CrossRef](#)]
20. Hoteit, H.; Firoozabadi, A. Compositional Modeling of Discrete Fractured Media without Transfer Functions by Discontinuous Galerkin and Mixed Methods. *SPE J.* **2006**, *11*, 341–352. [[CrossRef](#)]
21. Sun, J.; Schechter, D.; Huang, C.K. Grid Sensitivity Analysis and Comparison Between Unstructured Perpendicular Bisector and Structured Tartan/Local-Grid Refinement Grids for Hydraulically Fractured Horizontal Wells in Eagle Ford Formation with Complicated Natural Fractures. *SPE J.* **2016**, *21*, 2260–2275. [[CrossRef](#)]
22. Xu, Y.; Sepehrnoori, K. Development of An Embedded Discrete Fracture Model for Field-Scale Reservoir Simulation with Complex Corner-Point Grids. *SPE J.* **2019**, *24*, 1552–1575. [[CrossRef](#)]
23. Xu, Y.; Cavalcante Filho, J.S.A.; Yu, W.; Sepehrnoori, K. Discrete-Fracture Modeling of Complex Hydraulic-Fracture Geometries in Reservoir Simulators. *SPE Reserv. Eval. Eng.* **2017**, *20*, 403–422. [[CrossRef](#)]
24. Xu, Y.; Yu, W.; Sepehrnoori, K. Modeling Dynamic Behaviors of Complex Fractures in Conventional Reservoir Simulators. *SPE Reserv. Eval. Eng.* **2019**, *22*, 1110–1130. [[CrossRef](#)]
25. Leines Artieda, J.A. Discrete Fracture Network Modeling and Simulation Using EDFM. Master’s Thesis, The University of Texas at Austin, Austin, TX, USA, 2020.

**Disclaimer/Publisher’s Note:** The statements, opinions and data contained in all publications are solely those of the individual author(s) and contributor(s) and not of MDPI and/or the editor(s). MDPI and/or the editor(s) disclaim responsibility for any injury to people or property resulting from any ideas, methods, instructions or products referred to in the content.